increase in field gradient (for example, five times larger) will dramatically speed up the acquisition time and thereby enable two- and three-dimensional imaging applications. (Because we average signal energy, rather than amplitude, the averaging time will decrease as the inverse fourth power of the gradient in the limit of low signal-to-noise ratio.) If the measurement time can be reduced below τ_m, real-time readout of the spin quantum state will become possible, enabling a wide variety of quantum measurement experiments. For molecular imaging applications, extension to single nuclear spin detection is necessary, but this will require a roughly 1,000-fold improvement in magnetic moment sensitivity. Considering that the present experiment represents a sensitivity improvement of 10^7 times over the original MRFM experiment[29], the remaining required improvement does not seem out of the question, especially since there is still considerable leeway for increasing the field gradient and lowering the operating temperature. □

Received 16 April; accepted 17 May 2004; doi:10.1038/nature02658.

1. Ciobanu, L., Seeber, D. A. & Pennington, C. H. 3D MR microscopy with resolution 3.7 μm by 3.3 μm by 3.3 μm. *J. Magn. Reson.* **158,** 178–182 (2002).
2. Blank, A., Dunnam, C. R., Borbat, P. P. & Freed, J. H. High resolution electron spin resonance microscopy. *J. Magn. Reson.* **165,** 116–127 (2003).
3. Sidles, J. A. Folded Stern-Gerlach experiment as a means for detecting nuclear magnetic resonance in individual nuclei. *Phys. Rev. Lett.* **68,** 1124–1127 (1992).
4. Sidles, J. A. *et al.* Magnetic resonance force microscopy. *Rev. Mod. Phys.* **67,** 249–265 (1995).
5. DiVincenzo, D. P. Two-bit gates are universal for quantum computation. *Phys. Rev. A.* **51,** 1015–1022 (1995).
6. Berman, G. P., Doolen, G. D., Hammel, P. C. & Tsifrinovich, V. I. Solid-state nuclear-spin quantum computer based on magnetic resonance force microscopy. *Phys. Rev. B* **61,** 14694–14699 (2000).
7. Stowe, T. D. *et al.* Attonewton force detection using ultrathin silicon cantilevers. *Appl. Phys. Lett.* **71,** 288–290 (1997).
8. Chui, B.W. *et al.* Mass-loaded cantilevers with suppressed higher-order modes for magnetic resonance force microscopy. *Technical Digest 12th Int. Conf. on Solid-State Sensors and Actuators (Transducers'03)* 1120–1123 (IEEE, Piscataway, 2003).
9. Stipe, B. C. *et al.* Electron spin relaxation near a micron-size ferromagnet. *Phys. Rev. Lett.* **87,** 277602 (2001).
10. Mozyrsky, D., Martin, I., Pelekhov, D. & Hammel, P. C. Theory of spin relaxation in magnetic resonance force microscopy. *Appl. Phys. Lett.* **82,** 1278–1280 (2003).
11. Berman, G. P., Gorshkov, V. N., Rugar, D. & Tsifrinovich, V. I. Spin relaxation caused by thermal excitations of high-frequency modes of cantilever vibration. *Phys. Rev. B* **68,** 094402 (2003).
12. Hannay, J. D., Chantrell, R. W. & Rugar, D. Thermal field fluctuations in a magnetic tip—implications for magnetic resonance force microscopy. *J. Appl. Phys.* **87,** 6827–6829 (2000).
13. Mamin, H. J., Budakian, R., Chui, B. W. & Rugar, D. Detection and manipulation of statistical polarization in small spin ensembles. *Phys. Rev. Lett.* **91,** 207604 (2003).
14. Castle, J. G., Feldman, D. W., Klemens, P. G. & Weeks, R. A. Electron spin-lattice relaxation at defect sites: E′ centers in synthetic quartz at 3 kilo-Oersteds. *Phys. Rev.* **130,** 577–588 (1963).
15. Albrecht, T. R., Grütter, P., Horne, D. & Rugar, D. Frequency modulation detection using high-Q cantilevers for enhanced force microscope sensitivity. *J. Appl. Phys.* **69,** 668–673 (1991).
16. Slichter, C. P. *Principles of Magnetic Resonance*, 3rd edn, 20–24 (Springer, Berlin, 1990).
17. Berman, G. P., Kamenev, D. I. & Tsifrinovich, V. I. Stationary cantilever vibrations in oscillating-cantilever-driven adiabatic reversals: Magnetic-resonance-force-microscopy technique. *Phys. Rev. A.* **66,** 023405 (2002).
18. Berman, G. P., Borgonovi, F., Goan, H.-S., Gurvitz, S. A. & Tsifrinovich, V. I. Single-spin measurement and decoherence in magnetic-resonance force microscopy. *Phys. Rev. B* **67,** 094425 (2003).
19. Brun, T. A. & Goan, H.-S. Realistic simulations of single-spin nondemolition measurement by magnetic resonance force microscopy. *Phys. Rev. A.* **68,** 032301 (2003).
20. Davenport, W. B. & Root, W. L. *An Introduction to the Theory of Random Signals and Noise* 104 (McGraw-Hill, New York, 1958).
21. Ting, M., Hero, A.O., Rugar, D., Yip, C.-Y. & Fessler, J.A. Electron spin detection in the frequency domain under the interrupted oscillating cantilever-driven adiabatic reversal (iOSCAR) protocol. Preprint at http://xxx.lanl.gov/abs/quant-ph/0312139 (2003).
22. Manassen, Y., Hamers, R. J., Demuth, J. E. & Castellano, A. J. Direct observation of the precession of individual paramagnetic spins on oxidized silicon surfaces. *Phys. Rev. Lett.* **62,** 2531–2534 (1989).
23. Durkan, C. & Welland, M. E. Electronic spin detection in molecules using scanning-tunneling-microscopy-assisted electron-spin resonance. *Appl. Phys. Lett.* **80,** 458–460 (2002).
24. Wrachtrup, J., von Borczyskowski, C., Bernard, J., Orritt, M. & Brown, R. Optical-detection of magnetic resonance in a single molecule. *Nature* **363,** 244–245 (1993).
25. Köhler, J. *et al.* Magnetic resonance of a single molecular spin. *Nature* **363,** 242–244 (1993).
26. Jelezko, F. *et al.* Single spin states in a defect center resolved by optical spectroscopy. *Appl. Phys. Lett.* **81,** 2160–2162 (2002).
27. Elzerman, J. M. *et al.* Single shot read-out of an individual electron spin in a quantum dot. *Nature* (in the press).
28. Jiang, H.-W., Xiao, M., Martin, I. & Yablonovitch, E. Electrical detection of electron spin resonance of a single spin in the SiO_2 of a Si field effect transistor. *Nature* (in the press).
29. Rugar, D., Yannoni, C. S. & Sidles, J. A. Mechanical detection of magnetic resonance. *Nature* **360,** 563–566 (1992).

Supplementary Information accompanies the paper on **www.nature.com/nature**.

Acknowledgements We thank J. Sidles, A. Hero, M. Ting, G. Berman, I. Martin, C. S. Yannoni and T. Kenny for discussions, and D. Pearson, Y. Hishinuma, M. Sherwood and C. Rettner for technical assistance. This work was supported by the DARPA Three-Dimensional Atomic-Scale Imaging programme administered through the US Army Research Office.

Competing interests statement The authors declare that they have no competing financial interests.

Correspondence and requests for materials should be addressed to D.R. (rugar@almaden.ibm.com).

Formation of zirconium metallic glass

Jianzhong Zhang & Yusheng Zhao

LANSCE Division, Los Alamos National Laboratory, Los Alamos, New Mexico 87545, USA

Bulk metallic glasses are commonly produced by the rapid cooling of liquid alloys[1]. They have emerged over the past decade as a novel class of materials, with attractive properties and technological promise[1,2]. The bulk metallic glasses so far produced contain three or more component elements[3,4]. These complex compositions are necessary to frustrate the crystallization of the liquid melt on cooling, but can also lead to phase separation, which is detrimental to the thermal and mechanical properties of metallic glasses[5–8]. Here we report, using X-ray diffraction measurements, the formation of a bulk metallic glass from elemental zirconium at high static pressures and low temperatures (relative to its melting temperature at atmospheric pressure). Amorphous zirconium can be recovered at ambient conditions and demonstrates a superior thermal stability compared to amorphous alloys[3,9], which could lead to new high-temperature applications of amorphous metals.

In multi-component systems, glass-forming ability (GFA) is viewed as the resistance to precipitation of crystalline phases from supercooled liquid metals[10], and alloys with high GFA all have three common features[3,4]: (1) they consist of at least three components; (2) there is significant mismatch of the atomic size of the constituent elements; and (3) there are negative heats of mixing among the major alloying elements. Addition of elements that are chemically and topologically different from the other species not only creates an energy barrier for nuclei to form but also effectively increases melt viscosity or fragility, which results in a reduced rate of both nucleation and growth and an increase in GFA. The production of bulk glassy materials in pure metals, however, remains a long-standing scientific curiosity and technological interest. The difficulties arise from the facts that the equilibrium melt viscosity of pure metals is three orders of magnitude smaller than that of amorphous alloys[11] and that current technology has yet to reach a cooling rate in excess of the 10^{10} °C s^{-1} that is needed to make pure metals amorphous[12].

We studied zirconium metal at pressures and temperatures up to 17 GPa and 1,000 °C, using energy-dispersive synchrotron X-ray diffraction and time-of-flight neutron scattering. In X-ray diffraction experiments, we used both DIA-type[13] and T-cup[14] large-volume high-pressure apparatus installed at Brookhaven and Argonne National Laboratories. Neutron scattering experiments were performed using a high-pressure/high-temperature (high *P–T*) cell assembly[15] in a TAP-98 toroidal-anvil press at Los Alamos Neutron Scattering Center. The starting sample of zirconium has a close-packed hexagonal structure (α-phase) and is of extremely high purity, with 35 p.p.m. Hf, less than 25 p.p.m. of C, N and Al,

and less than 50 p.p.m. of O, V and Fe. The zirconium samples were placed in boron nitride and/or NaCl capsules, with NaCl used as an internal pressure standard[16].

Both X-ray and neutron diffraction experiments reveal that the zirconium metal is in crystalline forms at pressures and temperatures up to 4.3 GPa and 900 °C. The formation of amorphous zirconium was first observed when ω-phase (a hexagonal structure but not close-packed) was heated to 650 °C at 5.3 GPa (Figs 1 and 2). The lower bound for glass formation is therefore bracketed between pressures of 4.3 and 5.3 GPa. Upon cooling, we observed crystallization of ω-phase from amorphous zirconium at 4.8 GPa and 450 °C, indicating that the crystalline–glass transformation is reversible at this *P*–*T* condition (Fig. 2). When zirconium metal was heated at higher pressures of 6.4 GPa and 8.6 GPa in two different experiments, glass formation was observed at 700 °C and 625 °C, respectively, and the glass was stable on further heating to 1,000 °C (Figs 1 and 3). In both experiments, the transformation sequence is from ω-phase to β-phase (a body-centred cubic, high-temperature phase), and from β-phase to amorphous phase. The temperature interval between first appearance of β and first appearance of amorphous phase is less than 25 °C. Upon slow cooling, we did not observe crystallization of either ω- or β-phase even at room temperature, indicating an irreversible process for glass formation in zirconium metal. These findings demonstrate that pressure plays a critical role in both formation and reversibility of amorphous zirconium. From another perspective, we can conclude that the irreversible formation of amorphous zirconium seems to occur only when glass is formed from the β-phase.

To further explore effect of pressure on the GFA, we performed an additional experiment at 14–17 GPa. We observed the transformation from ω-phase to β-phase between 500 and 600 °C; upon further heating, however, zirconium metal is only partially transformed to an amorphous phase at 750 °C and 14.5 GPa, and the diffraction pattern is dominated by the β-phase. Compared with our experimental results at lower pressures (Fig. 1), these observations tend to suggest that zirconium metal has a diminishing GFA with increasing pressure between 9 and 15 GPa. The fully amorphous zirconium can therefore be formed in a limited pressure–temperature space. The glass-forming region needs to be more accurately determined to constrain the phase diagram for zirconium metal, as well as to provide a better understanding of glass-forming kinetics.

The glass formed at 8.6 GPa and temperatures above 625 °C (Fig. 3) was annealed up to 900 °C at pressures as low as 2.8 GPa to investigate the thermal stability of amorphous zirconium outside its formation *P*–*T* conditions (Fig. 4). At these experimental conditions, we did not observe the precipitation of any crystalline phase from amorphous zirconium. The glass formed at high pressure and temperature appears to have a superior thermal stability when compared to amorphous alloys formed from the conventional melting–cooling process, which typically start crystallization when annealed at temperatures between 450 and 500 °C (refs 3, 9). Whether amorphous zirconium shows a similar thermal behaviour at atmospheric pressure remains to be explored. As a final note on the stability, both energy and angle dispersive diffraction on the recovered zirconium sample shows patterns that are characteristic of an amorphous phase, but they do not reveal any diffraction lines of crystalline zirconium (Figs 2–4 and Supplementary Fig. 1). Both recovered and starting samples do not show any Raman shifts except for surface oxidation, indicating that the bulk zirconium sample remains in an elemental form at our experimental con-

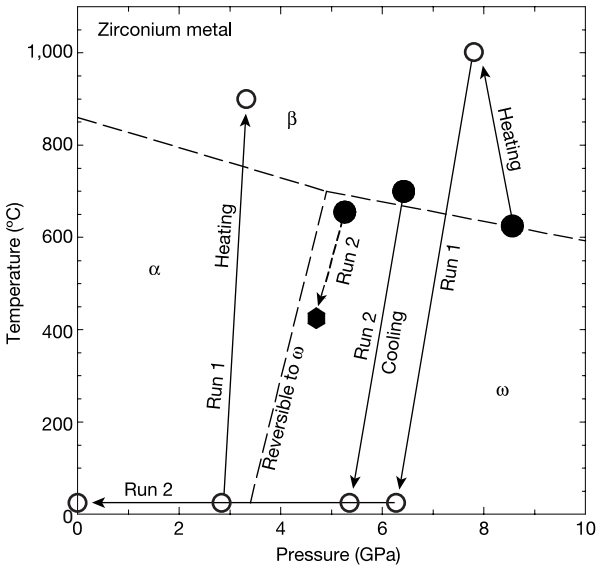

Figure 1 Glass-forming conditions and stability of amorphous zirconium. Formation of glass was observed in two independent experiments (runs 1 and 2). Filled circles refer to pressures and temperatures at which crystalline zirconium metal fully transformed into an amorphous phase on heating. The filled hexagon symbol corresponds to the conditions where the reversed transformation from glass to ω-phase was observed upon cooling. Arrows indicate the selected experimental *P*–*T* paths along which no precipitation of any crystalline phase was observed after the formation of amorphous zirconium, with open circles denoting a portion of data collected along the paths (see Fig. 4b for more detail for run 1). Experimental constraints on the phase diagram of zirconium metal (dashed lines) will be published elsewhere. A small amount of elemental addition has previously been demonstrated to significantly affect the glass-forming ability and physical properties in multi-component alloys[9]. Such effects in zirconium metal need to be explored as this study was carried out on zirconium specimens of ultra-high purity.

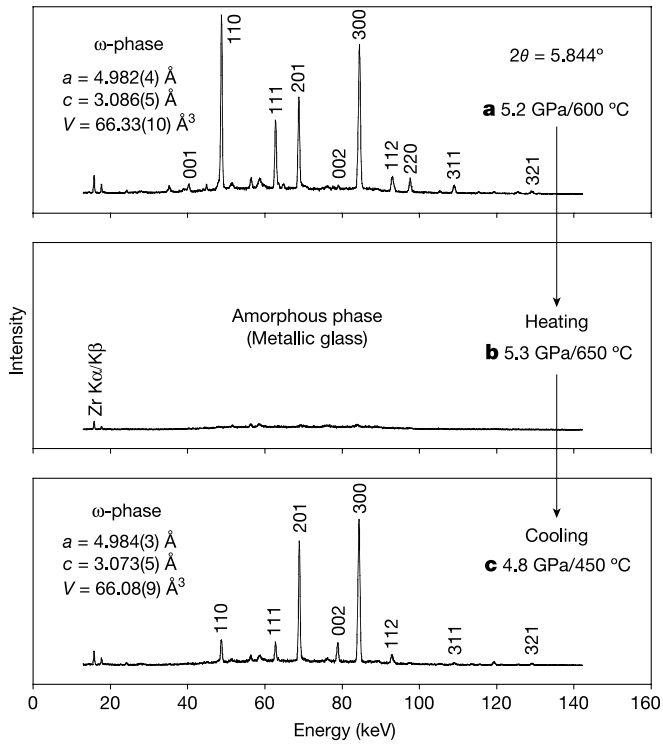

Figure 2 Selected synchrotron X-ray diffraction patterns showing a reversible transformation between ω-phase and amorphous phases of zirconium metal. Formation of a glass is identified by the disappearance of all diffraction peaks of ω-phase and by a significant reduction in the diffraction intensity (pattern **b**). Intensities have been normalized to the data acquisition time, and all three figures are plotted within an identical intensity range. The weak diffraction peaks observed in the amorphous phase are also present in all patterns collected in this experiment, and are from diffraction of materials surrounding the zirconium metal (see patterns **a** and **c**).

ditions. The microstructure and/or atomic scale structure of the recovered sample, however, need to be characterized by other experimental techniques, such as high-resolution transmission electron microscopy and neutron pair distribution function.

Phase transformations in zirconium metal have previously been studied at pressures and temperatures up to 6 GPa and 840 °C (ref. 17), and at 31–36 GPa up to 175 °C (refs 18, 19). The experimental conditions we found for the irreversible glass formation have therefore not been explored by any previous work. In addition, no theoretical calculations have predicted the instability of ω- and β-phases of zirconium metal relative to a solid amorphous phase[20,21]. At atmospheric pressure, zirconium metal melts at 1,855 °C; the melting curve at high pressures, however, is not known. But it is extremely unlikely that the observed glass formation can be attributed to the melting of zirconium metal at the experimental pressures, because this would require an unusually large negative dT/dP slope of $\sim$240 °C GPa^{-1}. The melting explanation is made more unlikely by the fact that the observed glass-forming temperature between 5 and 9 GPa only has a slightly negative dependence on pressure (Fig. 1). We therefore conclude that glass formation in zirconium metal by-passes the conventionally required liquid state, which represents a novel approach to making metallic glass. This experimental study presents (to our knowledge) the first finding that bulk metallic glass can be produced from a pure elemental metal.

Formation of an amorphous phase within a solid state by application of pressure has been found to be a phenomenon of widespread occurrence among condensed matter systems, such as silicates[22], ice[23] and alloys[24]. There are, however, major differences between these observations and the present findings. Pressure-induced amorphization is a process in which amorphous phase is formed because transformation from a crystalline solid to its high-pressure phase is kinetically hindered at ambient or low temperature[25]. In zirconium metal, formation of a glass occurs after α-phase transforms to its high-pressure and/or high-temperature phases. For pressure-induced amorphization, the glass would crystallize into its equilibrium, high-pressure phase when subjected to elevated temperatures. In zirconium glass, no precipitation of any crystalline phases was found at temperatures up to 1,000 °C. In fact, it is not known that there exists another high-temperature polymorph of zirconium metal except the β-phase. This leads to an unusual situation where amorphous zirconium would eventually 'melt' at somewhat higher temperatures, which could infer an extremely high thermal stability. Finally, no previous work has demonstrated that pure metals would undergo a pressure-induced amorphization.

Both measurements and molecular dynamics have revealed strong or anomalous softening of phonons along high symmetry directions in crystals of α-, ω- and β-phases of zirconium metal[26–28]. In particular, phonon anomalies have been observed in the dis-

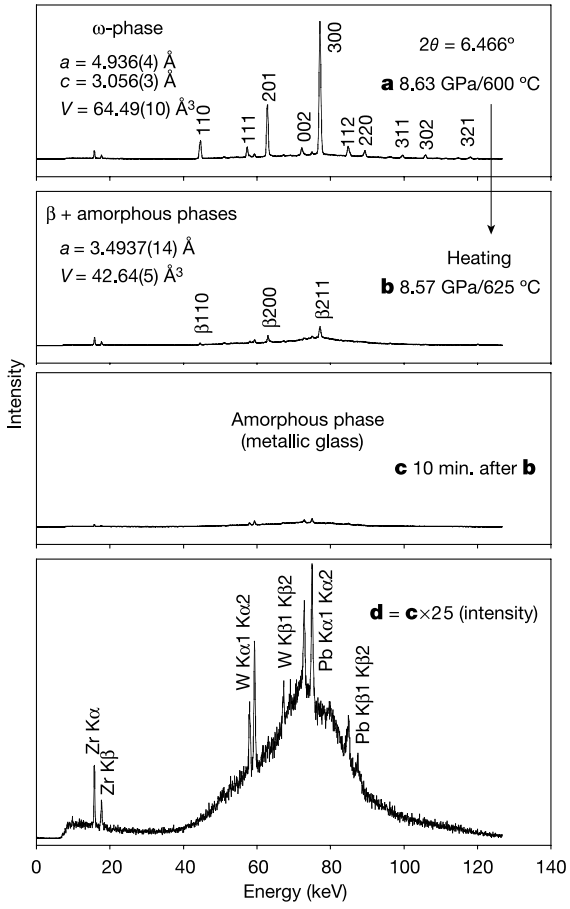

Figure 3 Selected diffraction patterns showing the ω–β phase transition and formation of glass from the β-phase of zirconium metal at 8.6 GPa. Pattern **d** is a blow-up of pattern **c**. It is well known that β-phase is formed by the splitting of alternating (001) planes along the *c* axis of an ω structure into two (111) planes of the β-phase. Therefore, diffraction pattern of the ω-phase contains all the diffraction lines of the β-phase and some characteristic lines resulting from its superlattice structure (patterns **b** and **c**). In this study and previous ones[18,19], the transition from ω-phase to β-phase is identified by the disappearance of the superlattice diffraction lines, (111), (002) and (112), of the ω-phase. Weak diffraction lines observed in all patterns are fluorescence peaks of tungsten, which was used to define collimation of the multi-element detector, and lead, which was used as a shielding material to avoid air scattering. For patterns **a**, **b** and **c**, intensities have been normalized to the data acquisition time, and all three figures are plotted within an identical intensity range.

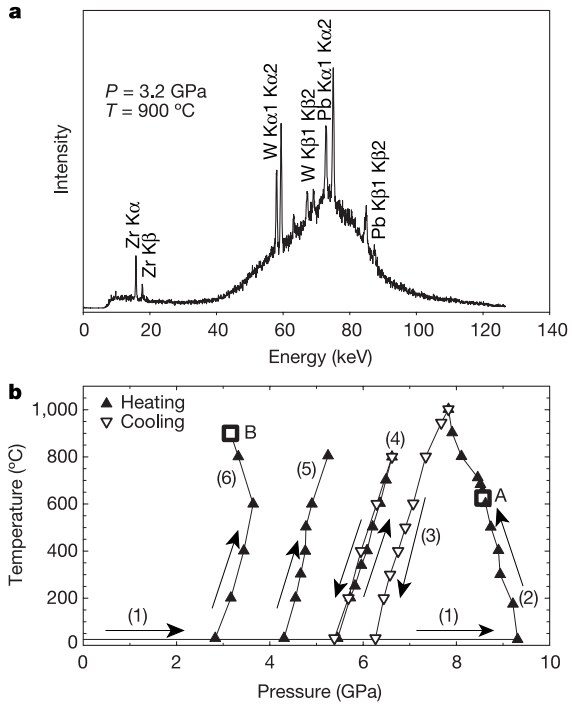

Figure 4 Experimental results demonstrating thermal stability/metastability of zirconium metallic glass. **a**, Diffraction pattern of glassy zirconium collected outside its forming conditions (Fig. 1). **b**, The *P*–*T* path for the experimental run 1. Open squares correspond to the conditions at which diffraction data were taken for Fig. 3d (point A) and Fig. 4a (point B). Numbers in parentheses and arrows indicate the sequential development of data collection in this experiment. After the first formation of amorphous zirconium at point A (8.57 GPa, 625 °C), the patterns collected in subsequent heating–cooling cycles at lower pressures and at the end of experiment are essentially identical to the ones shown in Fig. 3d and Fig. 4a.

persion curve of the high-temperature β-phase of zirconium at ambient pressure, which has been related to the β → ω and β → α phase transitions[26]. It is therefore possible that these phonon mode softenings may play a key role in the formation of zirconium metallic glass. Inelastic scattering at elevated pressure and temperature is needed to investigate the driving mechanisms for the present observations.

Liquid–liquid phase separation or decomposition of deeply undercooled metallic liquids is at present a major problem faced in the fundamental study and technological processing of bulk metallic glasses, even for extremely good glass-formers like Vit1 ($Zr_{41.2}Ti_{13.8}Cu_{12.5}Ni_{10}Be_{22.5}$) and Vit105 ($Zr_{52.5}Ti_5Cu_{17.9}Ni_{14.6}Al_{10}$) (refs 5–8). Similarly, decomposition happens when amorphous alloys are annealed at temperatures above the glass transition temperature[5], T_g. Experiments have revealed that such decomposition is responsible for the embrittlement of some bulk metallic glasses[1,5]. For mechanical applications, it is important to find metallic glasses that have higher thermal stability (that is, a smaller difference between the critical temperature[1], T_c, and T_g) and thus a lower probability of decomposition. As $T_c - T_g$ reduces, however, the amorphous alloys, such as derivatives of Vit1 and Vit105, tend to have a somewhat diminished GFA. We consider that the extraordinary GFA of pure zirconium metal, combined with its superior thermal stability, will overcome the problems that exist in amorphous alloys. In addition, the glass formed within a solid state may represent a distinct state of matter that may have other distinct properties yet to be explored, which may open new opportunities for research and development in the area of metallic glasses. □

Methods

Synchrotron X-ray experiments at high pressure and temperature were conducted on bulk, polycrystalline zirconium specimens of 1.0 mm diameter and 0.5 mm thickness, with the diffraction volume defined by 0.1 × 0.1 mm collimators. After observing the formation of amorphous zirconium, particular care was taken in our experiments, in that the formation of glassy zirconium was confirmed by collecting data at several different locations in the sample. The incident X-ray beam, however, is still too small compared to the bulk sample studied. In this regard, the GFA of bulk zirconium metal needs to be further studied by neutron diffraction.

In our high *P*–*T* neutron diffraction experiments, the cross-section of the incident neutron beam has a diameter of 5 mm, which is defined by cadmium and B_4C collimators. The time-of-flight neutron diffraction patterns were collected by eight detector banks that are available for TAP-98, at a fixed Bragg angle of $2\theta = 90°$. The experiments were performed on the polycrystalline zirconium specimens of ~100 mm^3 sample volume. This sample size, along with the current design of high-pressure cell, limits the experimental pressure to 5 GPa at high temperatures. So, unlike our X-ray diffraction experiments, our neutron diffraction experiments did not reach the *P*–*T* conditions needed for the glassy zirconium to form. These results are mainly used to constrain the α–β phase boundary, and will be published elsewhere.

Received 5 December 2003; accepted 4 June 2004; doi:10.1038/nature02715.

1. Loffler, J. F. Bulk metallic glasses. *Intermetallics* **11,** 529–540 (2003).
2. Johnson, W. L. Bulk glass-forming metallic alloys: science and technology. *MRS Bull.* **24,** 42–56 (1999).
3. Inoue, A. Stabilization of metallic supercooled liquid and bulk amorphous alloys. *Acta Mater.* **48,** 279–306 (2000).
4. Busch, R. The thermophysical properties of bulk metallic glass-forming liquids. *J. Miner. Metals Mater. Soc.* **52,** 39–42 (2000).
5. Miller, M. K. Decomposition of bulk metallic glasses. *Mater. Sci. Eng. A* **250,** 133–140 (1998).
6. Loffler, J. F. & Johnson, W. L. Model for decomposition and nano-crystallization of deeply undercooled $Zr_{41.2}Ti_{13.8}Cu_{12.5}Ni_{10}Be_{22.5}$. *Appl. Phys. Lett.* **76,** 3394–3396 (2000).
7. Kundig, A. A., Loffler, J. F., Johnson, W. L., Uggowitzer, P. J. & Thiyagarajan, P. Influence of decomposition on the thermal stability of undercooled Zr-Ti-Cu-Ni-Al alloys. *Scripta Mater.* **44,** 1269–1273 (2001).
8. Busch, R., Schneider, S., Peker, A. & Johnson, W. L. Decomposition and primary crystallization in undercooled $Zr_{41.2}Ti_{13.8}Cu_{12.5}Ni_{10}Be_{22.5}$ melts. *Appl. Phys. Lett.* **67,** 1544–1546 (1995).
9. Wang, W. H. *et al.* Role of addition in formation and properties of Zr-based bulk metallic glasses. *Intermetallics* **10,** 1249–1257 (2002).
10. Eckert, J., Mattern, N., Zinkevitch, M. & Seidel, M. Crystallization behavior and phase formation in Zr-Al-Cu-Ni metallic glass containing oxygen. *Mater. Trans.* **39,** 623–632 (1998).
11. Busch, R., Masuhr, A., Bakke, E. & Johnson, W. L. Bulk metallic glass formation from strong liquids. *Mater. Sci. Forum* **269,** 547–552 (1998).
12. Ashby, M. F. & Jones, D. R. *Engineering Materials 2: An Introduction to Microstructures, Processing and Design* (Pergamon, Oxford, 1986).
13. Weidner, D. J., *et al.* in *High-Pressure Research: Application to Earth and Planetary Sciences* (eds Syono, Y. & Manghnani, M. H.) 13–17 (Geophysics Monograph Series, Vol. 67, American Geophysical Union, Washington DC, 1992).
14. Vaughan, M. T. *et al.* T-cup: A new high-pressure apparatus for X-ray studies. *Rev. High Press. Sci. Technol.* **7,** 1520–1522 (1998).
15. Zhao, Y., Von Dreele, R. B. & Morgan, J. G. A high P-T cell assembly for neutron diffraction up to 10 GPa and 1500 K. *High Press. Res.* **16,** 161–177 (1999).
16. Decker, D. L. High-pressure equation of state for NaCl, KCl and CsCl. *J. Appl. Phys.* **42,** 3239–3244 (1971).
17. Jayaraman, A., Klement, W. & Kennedy, G. C. Solid-solid transition in titanium and zirconium at high pressures. *Phys. Rev.* **131,** 644–649 (1963).
18. Xia, H., Duclos, S. J., Ruoff, A. L. & Vohra, Y. K. New high-pressure phase transition in zirconium metal. *Phys. Rev. Lett.* **64,** 204–207 (1990).
19. Xia, H., Ruoff, A. L. & Vohra, Y. K. Temperature-dependence of the ω-bcc phase transition in zirconium metal. *Phys. Rev. B* **44,** 10374–10376 (1991).
20. Jona, F. & Marcus, P. M. Zirconium under pressure: Structure anomalies and phase transitions. *J. Phys. Condens. Matter* **15,** 5009–5019 (2003).
21. Ostanin, S. A. & Trubitsin, V. Y. Calculation of the P-T phase diagram of Zr in different approximations for the exchange-correlation energy. *Phys. Rev. B* **57,** 13485–13490 (1998).
22. Hemley, R. J., Jephcoat, A. P., Mao, H. K., Ming, L. C. & Manghnani, M. H. Pressure-induced amorphization of crystalline silica. *Nature* **334,** 52–54 (1988).
23. Mishima, O., Calvert, L. D. & Whalley, E. Melting of ice-I at 77 K and 10 Kbar: A new method of making amorphous solids. *Nature* **310,** 393–395 (1984).
24. Highmore, R. J. & Greer, A. L. Eutectics and the formation of amorphous alloys. *Nature* **339,** 363–365 (1988).
25. Richet, P. & Gillet, P. Pressure-induced amorphization of minerals: a review. *Eur. J. Miner.* **9,** 907–933 (1997).
26. Heiming, A. *et al.* Phonon-dispersion of the bcc phase of group-IV metals 2: Bcc zirconium, a model case of dynamic precursors of martensitic transitions. *Phys. Rev. B* **43,** 10948–10962 (1991).
27. Olijnyk, H. & Jephcoat, A. P. Effect of pressure on Raman phonons in zirconium metal. *Phys. Rev. B* **56,** 10751–10753 (1997).
28. Pinsook, U. & Ackland, G. J. Calculation of anomalous phonons and the hcp-bcc phase transition in zirconium. *Phys. Rev. B* **59,** 13642–13649 (1999).

Supplementary Information accompanies the paper on **www.nature.com/nature**.

Acknowledgements This work was performed under the auspices of the US Department of Energy with the University of California. The synchrotron X-ray diffraction experiments were conducted at X17B2 beamline of NSLS and BM-13 beamline of APS, operated by COMPRES and GESCARS, respectively.

Competing interests statement The authors declare that they have no competing financial interests.

Correspondence and requests for materials should be addressed to J.Z. (jzhang@lanl.gov).

Hydrological response to a seafloor spreading episode on the Juan de Fuca ridge

Earl Davis[1], Keir Becker[2], Robert Dziak[3], John Cassidy[1], Kelin Wang[1] & Marvin Lilley[4]

[1]*Pacific Geoscience Centre, Geological Survey of Canada, Sidney, British Columbia V8L 4B2, Canada*
[2]*Rosenstiel School of Marine and Atmospheric Science, University of Miami, Miami, Florida 33149, USA*
[3]*Oregon State University/NOAA, Hatfield Marine Science Centre, Newport, Oregon 97365, USA*
[4]*School of Oceanography, University of Washington, Seattle, Washington, 98195, USA*

Seafloor hydrothermal systems are known to respond to seismic and magmatic activity along mid-ocean ridges, often resulting in locally positive changes in hydrothermal discharge rate, temperature and microbial activity, and shifts in composition occurring at the time of earthquake swarms and axial crustal dike injections[1–10]. Corresponding regional effects have also been observed[11]. Here we present observations of a hydrological response to seafloor spreading activity, which resulted in a negative formation-fluid pressure transient during and after an earthquake swarm in the sediment-sealed igneous crust of the